JOURNAL OF
THE INTERNATIONAL ASSOCIATION
FOR SHELL AND SPATIAL
STRUCTURES

Prof. D. h-C Eng. E. TORROJA, founder

Vol. 65 (2024) No. 3
September n. 221
ISSN: 1028-365X

Journal

VOL. 65 (2024) No. 3
n. 221 September

contents

Announcements

Technical Papers

COVER*: Figure from paper by C. Wu, Q. Qing, Y. Pang and J. Gong*

IASS Secretariat: CEDEX-Laboratorio Central de Estructuras y Materiales
Alfonso XII, 3; 28014 Madrid, Spain
Tel: 34 91 3357465; Fax: 34 91 3357422; https://iass-structures.org
journal@iass-structures.org; iass@iass-structures.org
Printed by SODEGRAF ISSN:1028-365X Depósito legal: M. 1444-1960

IN-PLANE DESIGN OF NON-CIRCULAR TRIANGULATED TENSILE SPOKE WHEELS

Rodrigo MARTÍN-SÁIZ[1] and Blas HERRERA[2]

[1]PhD Architecture, Escola Tècnica Superior d'Arquitectura, Universitat Rovira i Virgili, Av. De la Universitat, 43204 Reus, Spain. rodrigo.martin@urv.cat
[2]ScD Mathematics, Departament d'Enginyeria Informàtica i Matemàtiques, Universitat Rovira I Virgili, Av.Països Catalans 26, 43007 Tarragona, Spain. blas.herrera@urv.cat

Editor's Note: Manuscript submitted 18 February 2023; revisions received 26 June 2023 and 05 February 2024; accepted 19 March 2024. This paper is open for written discussion, which should be submitted to the IASS Secretariat no later than March 2025.

DOI: https://doi.org/10.20898/j.iass.2024.005

ABSTRACT

This paper presents a new in-plane design of non-circular triangulated tensile spoke wheels with two perpendicular symmetry axes, like those used for roofing big sports stadiums, as well as a procedure to define such design. The proposed procedure describes how to define the in-plane shape and the necessary pre-stressing so that the outer ring behaves like a funicular polygon which has equal-length sides and is uniformly compressed. All in all, this procedure solves the problem of non-circularity of a triangulated spoke wheel by equalising the cross section sizing conditions of the outer ring to the sizing conditions that a circular structure would have.

Keywords: *Triangulated tensile spoke wheels, non-circular shape, homothetic deformation*

1. APPROACH

1.1. Introduction

Spoke-wheel-like roof structures are formed by pre-stressed spokes which are connected to inner tension rings and outer compression rings, where the supports are located. The spokes are usually organised into two layers: top and bottom. These two spoke layers are not parallel to each other, but usually converge at one of the rings. Thus, these structures can be classified into two subtypes: those which have two outer compression rings and one inner tension ring (Figure 1c), and those which have one outer compression ring and two tension inner rings (Figures 1a and 1b). In the former case, the two outer compression rings are separated by masts located at the outer end of the spokes. In the latter case, the masts are located between the two inner tension rings at the inner end of the spokes, and thus they are suspended in the air [1]. The profile of the spokes, biconcave (Figures 1b and 1c) or biconvex (Figure 1a), determines the use of intermediate ties or floating masts respectively between the inner and the outer ring. There is a third, less common subtype where the two spoke layers are crisscrossed between two outer compression rings and two inner tension rings (Figure 1d).

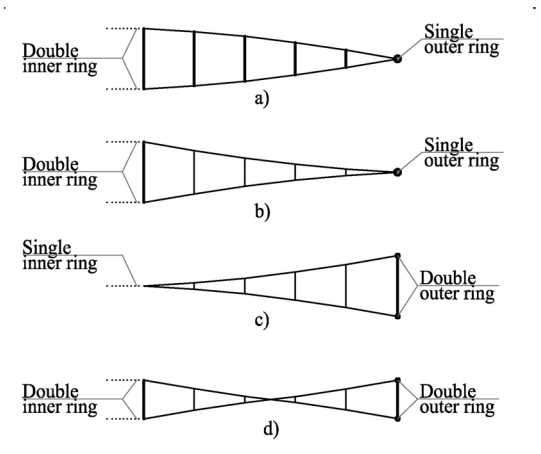

Figure 1: *Ring arrangements and spoke profiles*

If spans are long and live loads are small, the ratio between the self-weight and the whole of the loads of a spoke-wheel-like structure is usually much smaller than any other type of structure, especially with overhangs longer than 35 m [2].

The cross section sizing of the tensile spokes and inner tensile rings is only conditioned by the material's strength. This is why, if the material is very resistant to tension forces, it can have a very small cross section and the material consumption is kept to a minimum. Masts are jointed at their ends. This prevents bending moments and shear forces. These masts are slender and might suffer from buckling, however, they do not need a big cross section because the compression forces which they bear are relatively small. Therefore, the material consumption for masts is not often relevant. By contrast, the outer ring is subject to great compression forces. The variation of these forces around the ring's perimeter depends mainly on the variation of the curvature radius and the asymmetry of the live loads. Besides, the mismatch between the geometric shape of the outer ring and the in-plane reaction forces due to the spoke pre-stressing results in the occurrence of great bending moments and shear forces. For all these reasons, the cross section size of the outer ring (and also the material consumption) is usually much greater than for the rest of constructive elements of the wheel. Consequently, optimizing the design of the outer ring is essential in order to avoid compromising the efficiency of these structures.

If the spoke-wheel is inscribed in a circle, the optimum design is one in which the inner rings and the outer rings are shaped like regular polygons, with the spokes connected at the vertices. Thus, under permanent loads, if all the spokes are equally pre-stressed, the inner rings are only subject to tension forces and the outer rings are only subject to compression forces. Besides, these forces are uniform in all sides of the polygons. All in all, the inner and outer rings form funicular polygons (tensioned funicular polygons and uniformly compressed funicular polygons, respectively) resulting from the spokes reactions. Thus, under permanent loads (mainly the pre-stressing forces), the sizing conditions are the same on all the sides of the outer polygon, i.e., same buckling length and same compression force. At this point, it should be made clear that hereinafter in this paper the compression or tension rings having a polygonal geometry will be referred to as 'polygons', whereas the whole set of spokes plus the polygons will be referred to as 'wheel'.

If the wheel is inscribed in a non-circular shape, the optimum design is one which, under permanent loads (pre-stressing forces, mainly), manages to equalise the sizing conditions of all sides of the outer polygon, as happens if the wheel is inscribed in a circle. In order to achieve this objective, firstly, a non-regular polygon has to be defined which has equal-length sides, the vertices of which will connect to the spokes and to the vertical supports. Secondly, the spokes have to be distributed and pre-stressed in such a way that the inner and outer polygons are the funicular polygons resulting from the in-plane reactions of the spokes, and the outer polygon is uniformly compressed.

The problem of the mismatch between the funicular polygon and the geometric shape of the outer compression ring can be addressed in two ways: The first way involves designing a rigid element the geometric shape of which matches the funicular polygon resulting from the forces. The second way involves changing the geometric shape of the funicular polygon so that it matches the shape of the ring.

In the first instance, very often there is an excessive divergence between the optimal compression ring's shape and the building's shape. In such cases, minor changes can be made in order to approximate the ring's shape to a funicular polygon's shape, or in order to give the ring sufficient thickness so that a funicular polygon can be inscribed in it. However, both options are usually limited by the in-plane space which the ring can occupy. In the second instance, the funicular polygon is changed by adjusting the forces which define it, by means of pre-stressing.

For all of these reasons, the search of matching between the outer ring's shape and the funicular polygon's shape is the main problem in the design of non-circular spoke wheel roof structures. With regard to roof structures used in large sport arenas, on the one hand there is the need to place the compression ring along the stands perimeter, which is rarely circular in shape, and on the other hand, there is the need to approximate the compression ring's shape to a circle, which is the best known funicular polygon. This dual necessity almost always ends up in a solution which is not optimal for the ring's sizing. The roof of the Georgia Dome, designed by M. Levy and built in Atlanta in 1992, is an illustrative example of mismatch between the shape of the compression ring and the shape of a funicular polygon. Its oval shape is achieved by means of arc tangents of two circles having different radii. Despite the large cross section of the ring (8 m wide), it is not possible to inscribe a

funicular polygon in it. In the words of M. Levy: "*Obviously, in alternative configurations, as the oval shape tends toward a circle, moments would disappear as the circle becomes the funicular for the loads*" [3]. In the roof of the Commerzbank Arena (Deutsche Bank Park), designed by the German engineering and consulting firm Schlaich Bergermann Partner (SBP) and built in Frankfurt in 2005, the difference between the ring's shape and the stands perimeter is hidden inside a hollow cladding which is 8 m in width. This allows the structural geometry to more closely resemble the circular shape "*to create a viable structural system with moderate forces*" [4].

1.2. Aim and methodology

The purpose of this paper is to describe a new in-plane design of a triangulated spoke wheel which is non-circular in shape and has two perpendicular symmetry axes, as well as a procedure to define such design. The definition of the procedure is inherent to the new design. This procedure includes numerical methods specifically adapted for the form finding of the new design. Thus, a specific form finding method is defined in detail so that it can be included in a computer-aided design tool.

The in-plane behaviour of these structures due the pre-stressing forces is analogous to that produced in a flat wheel with a single layer of spokes. For this reason, in this paper, we use a flat wheel to analyse the in-plane behaviour of the structure. The aim is to obtain a design where the sizing conditions for the compression ring are optimal, as happens with wheels which are circular in shape.

In order to present the design procedure of the in-plane design of a triangulated spoke wheel, the starting point is to define the most relevant parameters with regard to the sizing of the compression ring. Next, there is a review of some outstanding examples of such structures, as well as the latest developments in the geometric design of rings and their relationship with pre-stressing forces. Then, the steps of the proposed design procedure are explained. For each step, systems of equations are presented and solving algorithms are proposed. Next, the limits and the scope of application of the design are defined. Lastly, the procedure is applied to a particular case, and a model is used in a structural analysis software which uses bar matrix calculation in order to compare the behaviour of the resulting structure with the behaviour predicted by the design procedure.

1.3. Background

Long span spoke wheel structures started being implement in the USA by the middle of last century, with the first projects by Lev Zetlin and Fred Severud [5]. These systems have gradually become the most common roof structures for grandstands in sports arenas [6]. Over the last three decades, the engineering firm SBP has designed more than twenty non-circular spoke wheel roof structures for large sport stadiums [7]. Several strategies and iterative methods have been used to achieve a better matching between the ring's shape and the pre-stressed cable reactions. Thanks to the improvement of these strategies and methods by SBP, it is now possible to design such structures having shapes increasingly different from the circle, without this significantly impacting on their sizing. In all these designs, the ring's radial deformation takes place freely, with no horizontal forces being transferred to the supports or the foundation. The inner and outer rings are concentric and they have a similar shape. The value of the radial cables pre-stressing varies inversely proportional to the curvature of the outer ring. Thus, the shape of the outer ring matches the shape of the funicular polygon of the tension forces on the spokes, which forces are projected on the wheel plane. For this reason, a mismatch between the compression ring's shape and the tension ring's shape increases the structure's sizing [8]. These criteria have helped to optimise the sizing conditions for the compression ring and its supports. Other structural engineers, such as M. Majowiecki, have also developed similar optimisation strategies when designing spoke wheel roof systems for large sports arenas [9].

Recent works deal the radial forces distribution so that an elliptical ring becomes funicular [10 and 11]. More recent form finding tools and methods make it possible to define funicular geometries of compressed or tensioned elements taking into account many different circumstances including spoke wheel systems [12-17]. Other recent studies specifically tackle the problem of designing spoke wheel structures with non-circular shapes [18-22] and the interaction between the tensile spokes and the rigid frames on the outer polygon [23 and 24]. This paper intends to delve into the design problem of non-circular wheels, applied to the specific case of triangulated arrangement of the spokes.

Typically, in-plane design of this type of structures has a radial arrangement of the spokes (Figure 2a) [4,

6-9]. This arrangement allows for an easier construction and more regular configuration of the membrane. In some cases, the spokes are forked at the outer end (Figura 2c) [25]; this variant has no obvious advantages, yet it increases the complexity of the construction. The crossed arrangement (Figure 2b), either two spoke layers with biconvex profile [26] or a single layer in the shape of a hyperbolic paraboloid [27], increases the stiffness in the wheel plane and solves the lateral stability of the masts, but involves greater complexity in membrane assembly configuration and of the construction. A radial arrangement in the upper layer combined with a triangulated arrangement in the lower layer (Figure 2d) [28] also increases stiffness in the wheel plane, but requires a V-shaped membrane between the spokes, with increases the roofing's surface area.

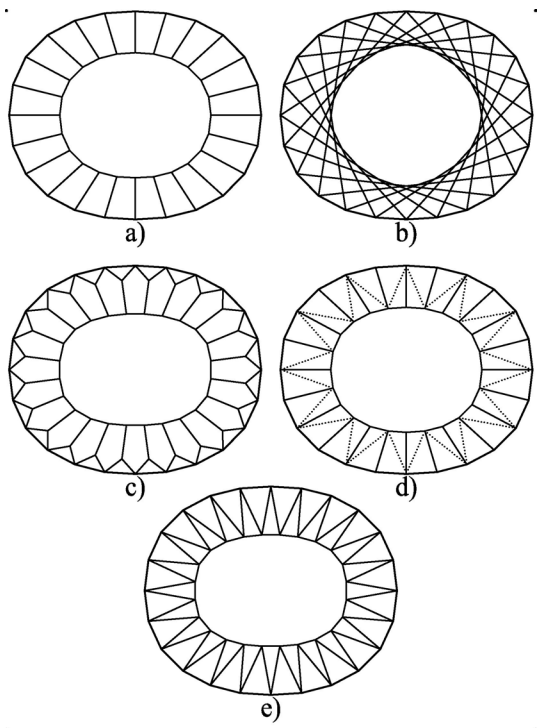

Figure 2: *Spoke arrangements in the wheel plane: a) radial arrangement, b) crossed arrangement, c) radial arrangement with forked spokes at the outer end, d) radial arrangement for the upper layer and triangulated arrangement for the lower layer, e) new design with triangulated spoke arrangement for both layers*

The triangulated arrangement (Figure 2e) proposed in this paper is an intermediate alternative between the simplicity of the radial arrangement and de complexity of the crossed arrangement. The triangulated arrangement also improves stiffness in the wheel plane without unduly increasing the complexity of the membrane assembly and configuration. Furthermore, the new design solves the lateral stability of the masts at the inner end of de spokes, between the inner polygons, without the use of bracing on the vertical plan.

The dilemma between the greater simplicity of the radial arrangement versus the greater stiffness and stability of the crossed-triangulated arrangement is an old discussion. Arguably the best example of this discussion is found in the comparison between the tensile dome models of D. Geiger [29], purely radial, and R. Buckminster Fuller [30], totally crossed-triangulated.

2. DEVELOPEMENT

2.1. Description of the design object: a flat non-circular triangulated tensile spoke wheel

The flat wheels which are proposed in this paper consist of an outer compression ring, an inner tension ring and tensile spokes which connect both rings. The behaviour of these flat wheels is analogous to the in-plane behaviour of pre-stressed spoke wheel roof structures used in big sports stadiums. The outer compression ring is shaped like a polygon with equal length sides and it is inscribed in a non-circular flat curve which is known beforehand, this curve having two perpendicular symmetry axes *X, Y* which will be Cartesian coordinate axes. As already explained in section 1, the equal sides criterion is necessary in order to equalise the buckling conditions of the sides. The inner tension ring is also a polygon with equal length sides, but it is not inscribed in a curve which is known beforehand. In this case, the equal-length-sides condition has not got a mechanical basis, but a purely geometric basis: the aim is to distribute the structure nodes in a way which is as uniform as possible. These two polygons have the same number of sides but they are not equally oriented, i.e., their vertices are offset (figure 3). The outer polygon has got four vertices which are located on the symmetry axes. These vertices are the limits of the maximum dimensions; i.e., the outer polygon is enclosed by the rectangle whose sides pass through those four vertices and are parallel to the Cartesian coordinate axes. On the contrary, the maximum dimensions of the inner polygon are limited by four of its sides; i.e., the inner polygon has four sides which make it to be enclosed by the rectangle whose sides contain such four sides and are parallel to the Cartesian coordinate axes. These four inner sides intersect with the symmetry axes at their mid-point. The vertical diameter and the horizontal diameter of the outer

polygon are known, because they are also the vertical diameter and the horizontal diameter of the inscribing curve. As for the inner polygon, only its horizontal diameter is known beforehand. The spokes connecting both polygons and the sides of the polygons form triangles due to the offset of the vertices. The bars forming these triangles are jointed at their vertices. Thus, four bars concur in each node of the structure: two adjacent sides of the polygon (either the outer polygon or the inner polygon) and two spokes (Figure 3). At this point, it must be made clear that the wheel consists of vertices (nodes) and of sides and spokes (bars). Hereinafter in this paper, we will use the terms 'vertices', 'sides' and 'spokes' when speaking about geometry, and the terms 'nodes' and 'bars' when speaking about the structure.

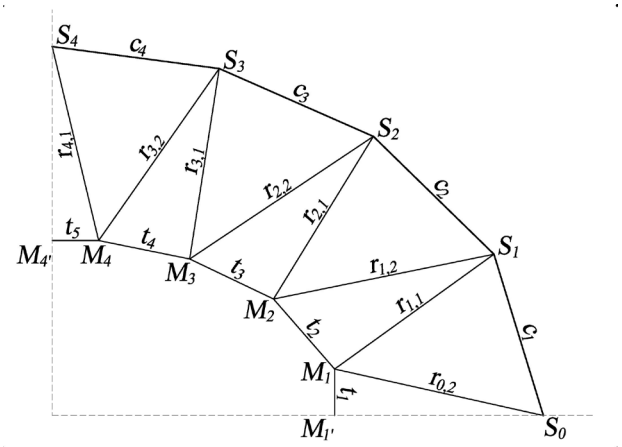

Figure 3: *Example of numbering of nodes and bars on a first quadrant of a spoke-wheel with n=4*

For the first quadrant of this wheel (Figure 3), the vertices are numbered in counterclockwise direction, starting with the vertex located on the symmetry axis X. Thus, the vertices of the outer polygon are S_0, S_1, S_2, …, S_n and the sides are c_1, c_2, c_3, …, c_n. In the same way, the vertices of the inner polygon are M_1, M_2, M_3, …, M_n and the sides are t_1, t_2, t_3, …, t_{n+1}. The sides t_1 y t_{n+1} determine the horizontal and vertical diameter of the inner polygon, and the ends of the inner polygon in this quadrant are the midpoints of these two sides. These ends are numbered in the same way as the closest vertex, with an added apostrophe, i.e., $M_{1'}$ and $M_{n'}$. The spokes are numbered according to the number of the outer polygon vertex where they meet (first subindex) and according to their position in relation to the same vertex, rotating in clockwise direction (second subindex), i.e., $r_{0,2}$, $r_{1,1}$, $r_{1,2}$, $r_{2,1}$, $r_{2,2}$, …, $r_{n,1}$ as shown in Figure 3. In addition, α_i, $\beta_{i,1}$, $\beta_{i,2}$ and ζ_i are the angles between the X-axe and the outer polygon sides, spokes and inner polygon sides respectively; γ_i is the angle between two sides of the outer polygon in a vertex and φ_i is the angle between the X-axe and the bisector of γ_i (figures 2, 3a and 3b).

If n is the number of sides of the outer polygon in a quadrant, $4n$ is the number of sides of the entire polygon (both, the inner polygon and the outer polygon), $8n$ is the total number of vertices, and $8n$ is also the total number of spokes. In other words, the total number of bars (sides and spokes) in a wheel is $16n$.

In an ideal pre-stressing state, the structure is homothetically deformed with regard to the initial structure, the homothetic center being at the crossing between the symmetry axes. In this ideal state, all the bars of the outer polygon are subject to the same compression force. Such pre-stressing state is caused by the introduction of an initial shortening of the tensile bars. This homothetic deformation is due to the pre-stressing of the wheel spokes. Thus, a homothetic in-plane deformation of the spoke wheel is only possible if both the outer polygon and the inner polygon are funicular polygons of the spoke reactions and all the bars of the outer polygon are subject to the same amount of axial force. This means that a specific geometric design is needed for this ideal state to take place.

2.2. Description of the design object: a flat non-circular tensile spoke wheel

The procedure to determine the outer polygon starts with a rectangle inscribing a super-ellipse [31], which is described by equation (1).

$$\left(\frac{x}{a}\right)^w + \left(\frac{y}{b}\right)^w = 1 \qquad (1)$$

…where a is half of the longer side of the rectangle, and b is half of the shorter side of the rectangle.

The 4-centered ovals and the 8-centered ovals are the most typical curves that describe the shape of the stands of large sports stadiums. The 4-centered ovals are defined by six parameters and the 8-centered ovals are defined by eleven parameters. It is possible to find a super-ellipse very close to any of these two types of ovals by varying its three parameters: a, b and w. Thus, we can define 4-centered ovals or 8-centered ovals in the same way with only three parameters. Following this, we can establish comparisons between them taking into account their mechanical behaviour (see section 2.4) or the

geometric limits of this design (see section 2.5), simply by varying *b/a* or *w*.

The super-ellipse is particularly interesting when designing roof structures for large sport arenas with grandstands surrounding a rectangular playfield. Figure 4 shows the schematic representation of stands around a rectangular pich, considering a super-ellipse with different exponents *w*. The greater *w* is, the better the shape of the stands matches the shape of the pitch.

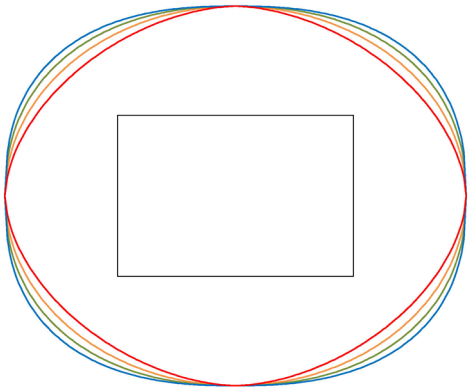

Figure 4: *Schematic representation of a rectangular pitch with surrounding super-elliptical stands, considering* w=*1.75 (red),* w=*2.00 (orange),* w=*2.25 (green) and* w=*2.50 (blue)*

The linear distance between two points of the curve, S_i and S_{i-1}, is calculated by means of the following equation (2):

$$L_i = \sqrt{\left(x_i - x_{i-1}\right)^2 + \left(y_i - y_{i-1}\right)^2}\,; i = 1 \div n \qquad (2)$$

Throughout the text of this paper, the notation means that from 1 to *n*, incrementing 1 by 1.

The problem of dividing the quadrant of the super-ellipse into *n* sides of equal length is defined by the system formed by equations 1 and 2. This system is solved by iteration. In a first approximation, $x_{i,0} = cos\left((\pi/2)i/n\right)$ is calculated, where $i = 1 \div n$. The values found are substituted into equation 1. Thus, we have obtaining the coordinates of the process starting point. Next, the length Li of each part is calculated; the average length $\overline{L} = (\sum L_i)/n$ is also calculated, and the ratio $\lambda_i = L_i/\overline{L}$ for each length is also calculated. The difference between the values of the *x*-coordinate at the ends of each resulting side is then changed in inverse proportion to each ratio, i.e. $x_{i+1,1} - x_{i,1} = \left(x_{i+1,0} - x_{i,0}\right)/\lambda_i$ .The ordinate values $y_{i,1}$ and the lengths are calculated again, and this iterative process is repeated until for each ratio λ_i, a value is obtained which is less than a tolerance value, i.e., until the error is less than a previously established value, $\tau_i = |1 - \lambda_i| \le 10^{-3}$. A smaller error in this process would not mean a higher accuracy in determining other parameters used in further calculations, since the error only affects the side length of the outer polygon. The iteration is convergent in all cases that were numerically solved in this paper. All thes cases were in the ranges $4 \le n \le 8$, $0.75 \le b/a \le 1.00$ and $1.75 \le w \le 2.50$. This numerical process y very easy to program and that is why it was implemented. In general, the reader could use any Other method that is convergent.

In order not to confuse the coordinates of the outer polygon vertices with the coordinates of the inner polygon vertices (which are defined later), (x_i, y_i) are renamed as (a_i, b_i), so that the semiaxes *a* and *b* of the super-ellipse are the coordinates a_0 and b_n for the vertices in the first quadrant of the outer polygon.

2.3. Shape of the inner polygon and arrangement of the spokes

The shape of the inner polygon depends on three conditions: the external equilibrium of the quadrant of the spoke-wheel, the internal equilibrium of its nodes and some additional, non-mechanical condition that allows defining a determined system of equations. In this case, we define this additional and non-mechanical condition is the equal length of its sides. I.e. there are many inner polygons that are funicular polygons of the same forces of which the outer polygon is also a funicular polygon, but only one of them has sides of equal lengths.

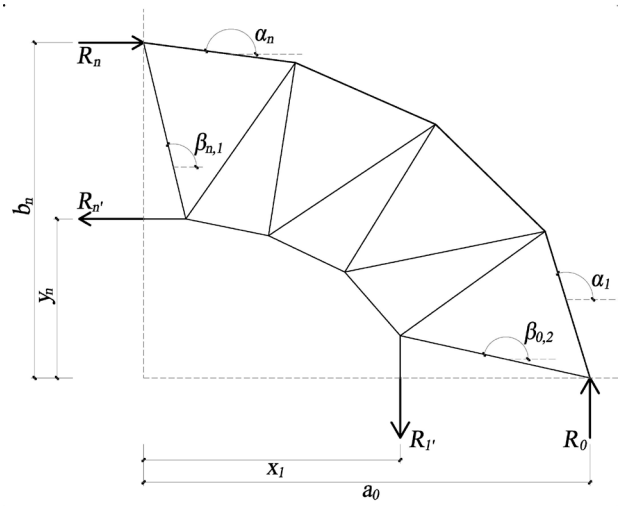

Figure 5: *Equilibrium reactions in the wheel's first quadrant*

Thus, we define the external equilibrium conditions of the wheel's first quadrant (3, 4 and 5), (Figure 5).

$$R_{n'} - R_n = 0 \tag{3}$$

$$R_{1'} - R_0 = 0 \tag{4}$$

$$R_n y_n + R_0 a_0 - R_n b_n - R_0 x_1 = 0 \tag{5}$$

After that, we define the equilibrium conditions of the inner polygon (6-9), (Figure 6b):

$$R_{1'} - N_1 = 0 \tag{6}$$

$$R_{n'} - N_{n+1} = 0 \tag{7}$$

$$N_{i+1}\cos\zeta_{i+1} + P_{i,1}\cos\beta_{i,1} + P_{i-1,2}\cos\beta_{i-1,2} - N_i\cos\zeta_i = 0, i = 2 \div n \tag{8}$$

$$N_{i+1}\sin\zeta_{i+1} + P_{i,1}\sin\beta_{i,1} + P_{i-1,2}\sin\beta_{i-1,2} - N_i\sin\zeta_i = 0, i = 2 \div n \tag{9}$$

…and the outer polygon taking into account an uniform compression force (N) (10-15), (Figure 6a):

$$R_0 - N\left(\sin\alpha_1 + \cos\left(\frac{\gamma_0}{2}\right)\tan\beta_{0,2}\right) = 0 \tag{10}$$

$$R_n - N\left(-\cos\alpha_n + \frac{\cos\left(\frac{\gamma_n}{2}\right)}{\tan\left(\beta_{n,1}\right)}\right) = 0 \tag{11}$$

$$P_{i,1} - P_{i,2}\frac{\sin\left(\varphi_i - \beta_{i,2}\right)}{\sin\left(\beta_{i,1} - \varphi_i\right)} = 0, i = 1 \div n-1 \tag{12}$$

$$P_{i,2} - \frac{2N\cos\left(\frac{\gamma_i}{2}\right)}{\cos\left(\varphi_i - \beta_{i,2}\right) + \frac{\sin\left(\varphi_i - \beta_{i,2}\right)}{\tan\left(\beta_{i,1} - \varphi_i\right)}} = 0, i = 1 \div n-1 \tag{13}$$

$$P_{n,1} - N\frac{\cos\left(\frac{\gamma_n}{2}\right)}{\sin\beta_{n,1}} = 0 \tag{14}$$

$$P_{0,2} - N\frac{\cos\left(\frac{\gamma_0}{2}\right)}{\sin\beta_{0,2}} = 0 \tag{15}$$

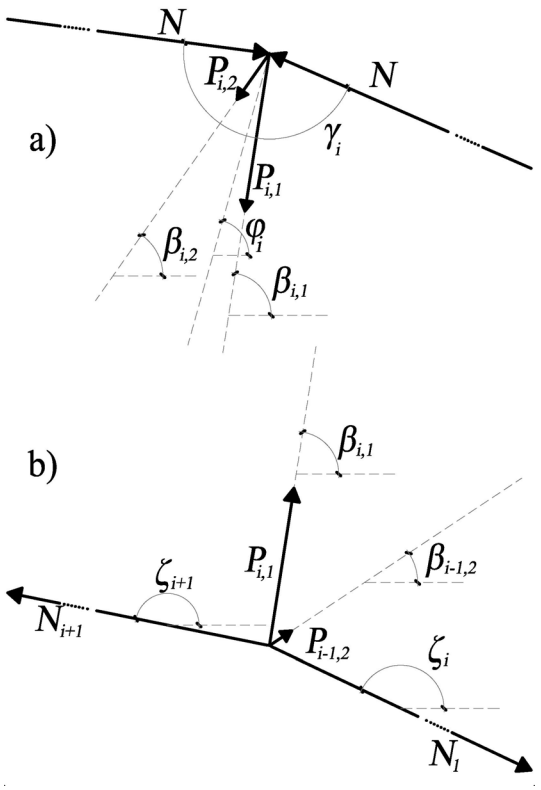

Figure 6: *a) Forces on a vertex of the outer polygon; b) forces on a vertex of the inner polygon*

Furthermore, there are some inherent geometry relationships between angles and lengths of the bars defined by equations (16-19), (figures 2, 3a and 3b).

$$\beta_{i,1} = \arccos\left(\frac{a_i - x_i}{\sqrt{\left(a_i - x_i\right)^2 + \left(b_i - y_i\right)^2}}\right), i = 1 \div n \tag{16}$$

$$\beta_{i,2} = \arccos\left(\frac{a_i - x_{i+1}}{\sqrt{\left(a_i - x_{i+1}\right)^2 + \left(b_i - y_{i+1}\right)^2}}\right), i = 1 \div n-1 \tag{17}$$

$$\beta_{0,2} = -\arccos\left(\frac{a_0 - x_1}{\sqrt{\left(a_0 - x_1\right)^2 + \left(b_0 - y_1\right)^2}}\right) \tag{18}$$

$$\zeta_i = \arccos\left(\frac{x_i - x_{i-1}}{\sqrt{\left(x_{i-1} - x_i\right)^2 + \left(y_{i-1} - y_i\right)^2}}\right), i = 2 \div n \tag{19}$$

At last, we define an additional condition. According this condition, all sides of the inner polygon must

have equal length (20a, 20b and 21). This condition makes it possible to arrange the spokes of the wheel in an orderly manner, but it does not imply any mechanical advantage.

$$\begin{aligned} L &= 2y_1 \\ L &= 2x_n \end{aligned} \qquad \text{(20a and 20b)}$$

$$L = \sqrt{\left(x_i - x_{i+1}\right)^2 + \left(y_i - y_{i+1}\right)^2} \qquad (21)$$
$$i = 1 \div n-1$$

Having defined the conditions to construct the inner polygon, we obtain a system Ω consisting of $8n+4$ equations; these equations are as follows: (3), (4), (5), (6), (7), (8) where $i=2\div n$, (9) where $i=2\div n$, (10), (11), (12) where $i=1\div n$-1, (13) $i=1\div n$-1, (14), 15), (16) where $i=1\div n$, (17) where $i=1\div n$-1, (18), (19) $i=2\div n$, (20a), (20b), and (21) where $i=1\div n$-1.

System Ω has got the same number of unknown variables $8n+4$, which are as follows: R_0, $R_{1'}$, R_n, $R_{n'}$, $P_{i,1}$ where $i=1\div n$, $P_{i,2}$ where $i=0\div n$-1, N_i where $i=1\div n+1$, $\beta_{i,1}$ where $i=1\div n$, $\beta_{i,2}$ where $i=0\div n$-1, $\zeta_{,i}$ where $i=2\div n$, x_i where $i=2\div n$, y_i where $i=1\div n$, and L.

System Ω depends on the following known parameters: n, x_1, $(a_i,\ b_i)$ where $i=0\div n$, N, γ_i where $i=0\div n$, φ_i where $i=1\div n$-1, α_1, α_n, $\zeta_1$and ζ_{n+1}.

This system could be simplified, but it is expressed like this because it offers the reader a clearer view of the involved mechanics and geometry.

Also, in addition to the equations which make up system Ω, the following inequalities (22a, 22b and 22c) must be fulfilled:

$$\begin{aligned} &\beta_{i,1} > \varphi_i > \beta_{i,2}, i = 1 \div n-1 \\ &0 < x_{i+1} < x_i, i = 1 \div n-1 \\ &0 < y_i < y_{i+1}, i = 1 \div n-1 \end{aligned}$$

(22a, 22b and 22c)

Next, we describe the method used to find the solution to Ω. As in the case of the outer polygon, an iterative method is used.

The variables of the system are renamed as follows: $L = z_1$, $y_1 = z_2$, $x_i = z_{2i-1}, y_i = z_{2i}$, where $i = 2 \div n$, $R_0 = z_{2n+1}$, $R_{1'} = z_{2n+2}$, $R_n = z_{2n+3}$, $R_{n'} = z_{2n+4}$, $N_i = z_{2n+4+i}$ where $i = 1 \div n+1$, $\beta_{i,1} = z_{3n+5+i}$ where $i = 1 \div n$, $\beta_{i,2} = z_{4n+6+i}$ where $i = 0 \div n-1$, $P_{i,1} = z_{5n+5+i}$ where $i = 1 \div n$, $P_{i,2} = z_{6n+6+i}$ where $i = 0 \div n-1$, $\zeta_i = z_{7n+5+i-1} = z_{7n+4+i}$ where $i = 2 \div n$, where $\{z_i\}_{i=1}^{i=8n+4}$.

The starting point $P_\alpha = \left(z_1, z_2, \ldots, z_{8n+4}\right)_\alpha \in \mathbb{R}^{8n+4}$ of our numerical calculations is generated from the input parameters (which are known beforehand). From a geometric point of view, this starting point is a first positioning of $\{z_i\}_{i=1}^{i=8n+4}$ in $\mathbb{R}^{8n+4}$. Let us remember that $\{z_i\}_{i=1}^{i=8n+4}$ are the $8n+4$ variables which are present in the $8n+4$ equations $\{f_i(z)\}_{i=1}^{i=8n+4}$ which make up system Ω. In order to determine P_α, we have the equations of the system and also the equations (23-28), based on which P_α can be generated.

$$L = \frac{x_1}{a_0}\sqrt{\left(a_1 - a_0\right)^2 + \left(b_1 - b_0\right)^2} \qquad (23)$$

$$y_1 = \frac{L}{2} \qquad (24)$$

$$x_n = \frac{L}{2} \qquad (25)$$

$$x_i = x_{i+1} + \frac{x_1}{a_0}\left(a_i - a_{i+1}\right), i = 2 \div n-1 \qquad (26)$$

$$y_i = y_{i-1} + \frac{x_1}{a_0}\left(b_i - b_{i-1}\right), i = 2 \div n-1 \qquad (27)$$

$$N_i = \frac{1}{2}\left(\begin{array}{l} \dfrac{N_{i+1}\cos\zeta_{i+1} + P_{i,1}\cos\beta_{i,1} + P_{i-1,2}\cos\beta_{i-1,2}}{\sin\zeta_i} \\ + \dfrac{N_{i+1}\sin\zeta_{i+1} + P_{i,1}\sin\beta_{i,1} + P_{i-1,2}\sin\beta_{i-1,2}}{\sin\zeta_i} \end{array}\right)$$

$$i = 2 \div n \qquad (28)$$

Once the starting point P_α of our method has been generated, an iterative calculation is performed in order to find the point $P_\mu = \left(z_1, z_2, \ldots, z_{8n+4}\right)_\mu \in \mathbb{R}^{8n+4}$. This second point P_μ is an approximation to the solution to Ω with tolerance $\tau = \sum_{i=1}^{8n+4}\left|f_i\left(P_\mu\right)\right| = \sum_{i=1}^{8n+4}\left|f_i\left(\left(z_1, z_2, \ldots, z_{8n+4}\right)_\mu\right)\right| < 10^{-2}$. A classical technique is used to find this second point. This technique involves an approximation

through level sets [32]. Although this is a classic method, a description is given below. This point P_μ is the starting point for the Newton-Raphson method, so that it converges to the point P_ω, which is the solution to Ω with the desired accuracy.

Thus, in order to find P_μ, a function $H:\mathbb{R}^{8n+4}\to\mathbb{R}$ is considered such that $H(z)=\sum_{i=1}^{8n+4}\left(f_i(z)\right)^2$ where $z=(z_1,z_2,...,z_{8n+4})$. The value of z which fulfils $H(z)=0$ will be the solution to system Ω. Our starting point P_μ is close to the solution $\omega\in\mathbb{R}^{8n+4}$ to system Ω. This solution is a strict minimum of $H(z)$.

Our calculations begin with the level set $S^{(0)}\subset\mathbb{R}^{8n+4}$ of function $H(z)$ at the starting point $z^{(0)}=P_\alpha$; i.e. $S^{(0)}\subset\mathbb{R}^{8n+4}$ is the set where the function H takes the constant value $H(P_\alpha)$. In the hypothetical case of H in $\mathbb{R}^2$, the level sets could be intuitively visualized as flattened curves which enclose ω. The graph of function H in $\mathbb{R}^3$ would be similar to a pit, the point $(\omega,H(\omega))=(\omega,0)\in\mathbb{R}^3$ being its bottom. Thus, the geometric method used to generate an approximation is described as follows: Using the direction of the straight line which is normal to level set $S^{(0)}$ (this level set has codimension 1), we move away from the starting point $z^{(0)}=P_\alpha$ until reaching another level set $S^{(1)}$ at another point $z^{(1)}$, in such a way that the contact between the normal straight line and the level set $S^{(1)}$ at point $z^{(1)}$ is tangential. We repeat this process starting with point $z^{(1)}$ and we find the point $z^{(2)}$, and so on. Since $H(z^{(0)})>H(z^{(1)})>H(z^{(2)})>|...,$ by using this method we will approximate point ω, the level of which is the lowest level of $H(z)$. This geometric iterative method is analytically expressed through the following iterative equation (29):

$$z^{(k+1)}=z^{(k)}-\lambda_k\nabla H\left(z^{(k)}\right) \qquad (29)$$

where ∇H is the gradient of H and $\lambda_k>0$ with k=0, 1, 2,... In this equation (29), λ_k has to be determined at every step.

In order to determine λ_k, we consider the function $\psi(\lambda):\mathbb{R}\to\mathbb{R}$ where $\psi(\lambda)=H\left(z^{(k)}-\lambda\nabla H\left(z^{(k)}\right)\right)$ This function is the level variation of function H along the straight line which is normal to level set $S^{(k)}$ at $z^{(k)}$. The value of λ_k should minimise $\psi(\lambda_k)$ because, when contact is tangential, the normal straight line does not cut through these level sets. However, instead of finding the true value of λ_k which minimises $\psi(\lambda)$, we calculate the following equation (30), which is an analytical approximation to λ_k. This analytical approximation is obtained by means of linear approximations using Taylor's formula.

$$\lambda_k=\frac{1}{2}\frac{f\left(z^k\right)Jf\left(z^{(k)}\right)Jf\left(z^{(k)}\right)^t f\left(z^{(k)}\right)^t}{f\left(z^k\right)Jf\left(z^{(k)}\right)Jf\left(z^{(k)}\right)^t Jf\left(z^{(k)}\right)Jf\left(z^{(k)}\right)^t f\left(z^{(k)}\right)^t} \qquad (30)$$

…where $f\left(z^k\right)=\left(f_1\left(z^{(k)}\right),...,f_{8n+4}\left(z^{(k)}\right)\right)$, and where $Jf\left(z^{(k)}\right)$ is the Jacobian matrix of $f(z)$ at $z^{(k)}$.

$$Jf\left(z^{(k)}\right)=\begin{pmatrix}\frac{\partial f_1}{\partial z_1} & \frac{\partial f_1}{\partial z_1} & ... & \frac{\partial f_1}{\partial z_{8n+4}}\\ \frac{\partial f_2}{\partial z_1} & \frac{\partial f_2}{\partial z_2} & ... & \frac{\partial f_2}{\partial z_{8n+4}}\\ . & . & ... & .\\ \frac{\partial f_{8n+4}}{\partial z_1} & \frac{\partial f_{8n+4}}{\partial z_2} & ... & \frac{\partial f_{8n+4}}{\partial z_{8n+4}}\end{pmatrix}\left(z^{(k)}\right)$$

It can also be proved that $\nabla H\left(z^{(k)}\right)=2f\left(z^{(k)}\right)Jf\left(z^{(k)}\right)$. Therefore, the formula of the iterative process is as follows (31):

$$z^{(k+1)}=z^{(k)}-\lambda_k 2f\left(z^{(k)}\right)Jf\left(z^{(k)}\right) \qquad (31)$$

where $z^{(0)}=P_\alpha$. The aim of this iterative process is to find $P_\mu=(z_1,z_2,...,z_{8n+4})_\mu\in\mathbb{R}^{8n+4}$ such that $\sum_{i=1}^{8n+4}\left|f_i(P_\mu)\right|=\sum_{i=1}^{8n+4}\left|f_i\left((z_1,z_2,...,z_{8n+4})_\mu\right)\right|<10^{-2}$. We do not pursue greater accuracy in this part of our calculations because the undulations of the level sets in the vicinity of ω (as a result of the functions $f_{6n+5+i},\ldots,f_{8n+4}$) make the linear approximation method unsuitable for the calculation of λ_k.

Since P_μ is close to the sought-after solution ω, we use the well-known Newton-Raphson method for solving systems of equations. As the starting point

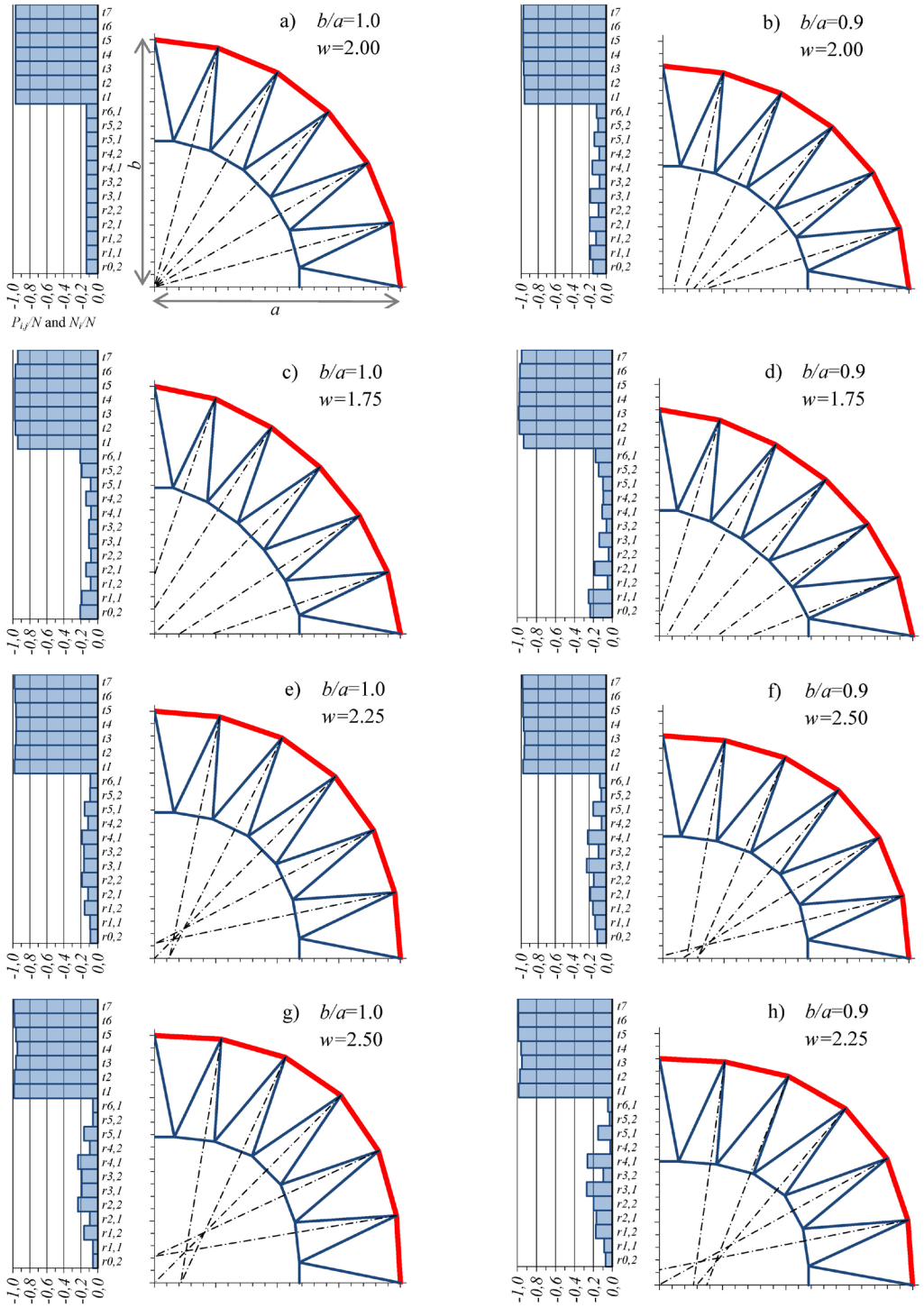

Figure 7: *In-plane resulting design of eight spoke-wheels considering* n=*6 and several parameters (*b/a *and* w*) of the super-ellipse. On the left of each wheel, the in-plane tension force distribution on spokes (*$P_{i,j}$/N*) and inner polygon (*N_i/N*)*

for this method we use P_μ. Thus we obtain the final solution $P_\omega = (z_1, z_2, \ldots, z_{8n+4})_\omega \in \mathbb{R}^{8n+4}$ to system Ω with tolerance $\tau = \sum_{i=1}^{8n+4} |f_i(P_\omega)| = \sum_{i=1}^{8n+4} |f_i((z_1, z_2, \ldots, z_{8n+4})_\omega)| = 10^{-10}$ ultimately reaching the desired accuracy.

2.4. Families of homothetic spoke-wheels

According to this method, we have solved the in-plane design for eight spoke-wheels considering n=6 and several different parameters of the inscribing super-ellipses (Figure 7). Each one of these figures represents, in fact, a family of homothetic spoke-wheels. As long as the same geometric proportions and the same relationships between forces are maintained, the spoke-wheel will deform homothetically. This issue is explained later.

The relative values of the tension forces on the spokes and on the inner polygon sides, $P_{i,j}/N$ and N_i/N respectively, are shown to the left of each figure. It is clear from the figure 7 that the in-plane forces distribution of the spokes are conditioned by the shape of the outer polygon. Thus, the difference between the tension forces of the spokes increases as the shape of the inscribing super-ellipse differs from the circumference (figure 7a).

Also, we can see in the figures 7a to 7h that the biggest tension forces of the spokes coincide with the zone maximum curvature of the super-ellipses: when w=1.75, near the symmetry axes; when w=2.00, near the X-axe; when w>2, between the two symmetry axes.

2.5. Maximal wheel depth and geometric scope

The inequality 22a limits possible solutions to those where all spokes are subject to tension forces. In other words, not all value combinations of the design input parameters (a_0, b_n, w, n and x_1) lead to a wheel where all spokes are subject to tension forces. Since there is an infinite number of possible combinations for the design input parameters, we have restricted the range of possible values with the following conditions: $0.75 \le b_n/a_0 \le 1$, and $1.75 \le w \le 2.5$. These intervals meet a criterion of reasonable design explained below. Thus, for each of these combinations we would obtain a minimum x_1 value for which $\beta_{i,1} = \varphi_i > \beta_{i,2}$ or $\beta_{i,1} > \varphi_i = \beta_{i,2}$ in at least one spoke of the wheel. Hereinafter, this minimum value is called $x_{1,lim}$ (Figure 8).

In contrast to the limits laid down by the aforementioned intervals, $x_{1,lim}$ is indeed a strict limit of x_1 below which we could not obtain a valid design. Then, the maximum wheel depth occurs when $x_1 = x_{1,lim}$ for a certain combination of a_0, b_n, w and n. Since $x1$ is an input parameter in the design process, the máximum depth measured along the X-axis whill be used $(a_0 - x_{1,lim})$ to limit the geometric scope of the method described in subsection 2.3.

Figure 8 shows that the relative distribution of tension forces ($P_{i,j}/N$) on the spokes becomes less uniform as the wheel depth increases. The maximum depth is reached when one of the spokes coincides with the bisector (highlighted in red in the figure) of the angle γ at the vertex of the outer polygon, i.e. when inequality 22a is no longer fulfilled. The adjacent spoke at the same vertex will then have zero tension.

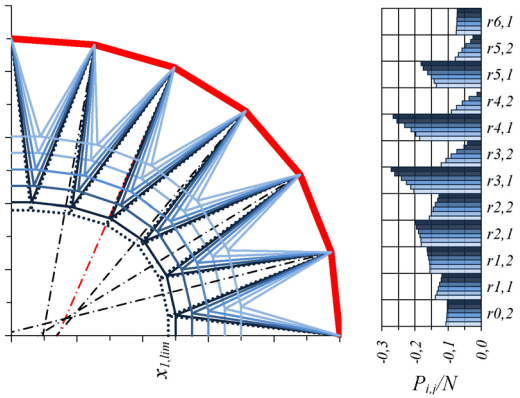

Figure 8: *On the left, in-plane design of six spoke wheels considering the same outer polygon and different values of* x_1 *until* $x_{1,\mathrm{lim}}$ *is reached. The right-hand side shows how the relative distribution of forces on the spokes varies as function of the wheel depth until* $P_{i,j}$ *is zero on one of the spokes, when* $x_{1,\mathrm{lim}}$ *is reached*

Figure 9 below shows the relative maximum wheel depth $(a_0 - x_{1,lim})/a_0$ along the X-axe dependent on the ratio of the semi-axes of the super-ellipse, for n=4, n=6 and n=8 taking into account forty-four different combinations values of b_n/a_0 and w. Analogous curves can be defined taking into account other different values of n.

It is clear from the curves of the figure 9 that the maximum depth along the X-axe is greater the more the super-ellipse resembles a circle. It is also clear that the greater n is, the smaller the maximum depth.

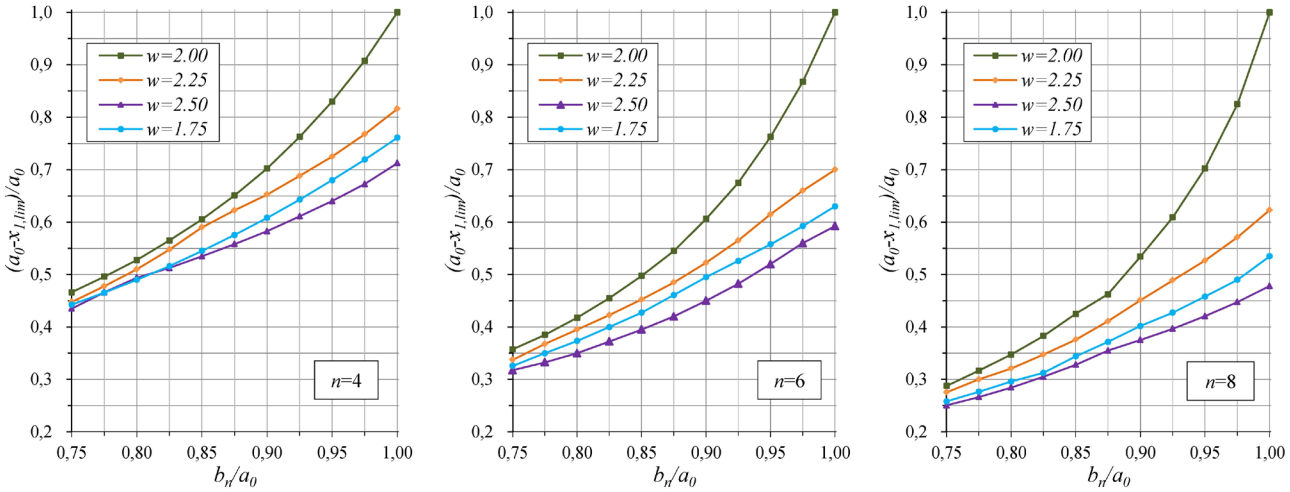

Figure 9: *Curves of maximal wheel depth along the* X*-axe dependent on the ratio* b_n/a_0 *and the exponent* w *of the super-ellipse, taking into account* n*=4, n=6 and n=8*

Thus, a reasonable wheel design is the one where the relative depth $(a_0 - x_1)/a_0$ is sufficiently similar to the design of roof structures such as are described in section 1 of this paper. These structures are meant for roofing stands with a ratio $0.75 \le b_n/a_0 \le 1$ and a depth $(a_0 - x_1) \ge 35$ m.

2.6. Homothetic in-plane deformation

As already explained earlier in this paper, the ideal behaviour of the outer polygon occurs when all its sides (which have the same length) are subject to the same compression force *N*. For this to happen, all the sides have to undergo the same unit shortening, according to the area of the cross section (*A*) and the elasticity modulus (*E*) of the material, typically steel. As a result of the homothetic deformation, a certain compression force can be related with a reduction factor (1-ε). This reduction factor should not be lower than (1-$\varepsilon_{y,c}$), where $\varepsilon_{y,c}$ is the yield strain of the outer polygon's material. Besides, other circumstances such as buckling or out-of-plane bending moments would further limit the capacity of the outer polygon to deform in its own plane. This is why, in general, this scale reduction factor can be expressed as (1-$k\varepsilon_{y,c}$), where *k* is a relative utilization of the yield strength on the outer polygon's material. This reduction factor should be defined on a case by case through a cross section sizing estimation process basis on the out-of-plane loads (self-weight, snow and wind loads) and the spoke's profiles [33].

Using a polar coordinates system (ρ,θ), when the entire structure is homothetically deformed, the in-plane distance $\rho(\theta)$ from the origin of the coordinate system (the center of the wheel) to each node is reduced by the proportion (1-$k\varepsilon_{y,c}$) (Figure 10). This makes it possible to determine the position ($x_{i,k}$, $y_{i,k}$) of each node of the deformed wheel according to the equation (32):

$$\begin{aligned} x_{i,k} &= \rho_i \left(1 - k\varepsilon_{y,c}\right) \cos\theta_i \\ y_{i,k} &= \rho_i \left(1 - k\varepsilon_{y,c}\right) \sin\theta_i \end{aligned} \qquad (32)$$

Next, each node's in-plane displacements due the homothetic deformation are calculated by means of equations (33a and 33b): The displacement of any other node between the inner and the outer polygons can be calculated by analogous equations.

$$\begin{aligned} \delta_{S,i} &= \sqrt{\left(a_i - a_{i,k}\right)^2 + \left(b_i - b_{i,k}\right)^2} \\ \delta_{M,i} &= \sqrt{\left(x_i - x_{i,k}\right)^2 + \left(y_i - y_{i,k}\right)^2} \end{aligned}$$

(33a and 33b)

Lastly, the pre-stressing of the tensile bars (the spokes and the sides of the inner polygon) is calculated. This is the pre-stressing which is needed for the wheel to deform homothetically. This pre-stressing is introduced by means of an initial shortening $\Delta L_{0,i}$.

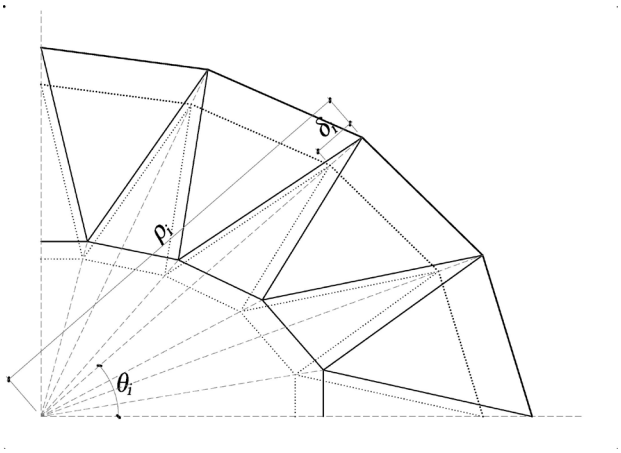

Figure 10: *Homothetic in-plane deformation of the wheel's first quadrant*

We consider now a non-flat spoke wheel. The inner polygons of these structures are usually contained in horizontal planes, parallels to those of the outer polygons. The initial shortening of these inner polygon bars is the difference between: a) the shortening that the bar would undergo as a result of the tension force N_i and its axial stiffness, and b) the shortening that the wheel really undergoes according to the homothetic deformation. Taking into account a symmetrical design regarding the horizontal plane of the outer polygon, this initial shortening is determined by the equation (34):

$$\Delta L_{0,i} = L_i \left(\frac{N_i}{2EA_i} - k\varepsilon_{y,c} \right) \tag{34}$$

… where A_i is the area of the cross section of the inner polygon.

The spokes of these structures are usually composed by two polygonal strings contained in a vertical plane. There are ties or floating masts between the two strings depending on the spoke profile, biconcave or biconvex respectively. The z coordinates of each string are defined from the length of the ties or floating masts. In order to define the initial shortenings of these strings, first of all we need calculate its length (35).

$$L_i = \sqrt{\left(x_1 - x_2\right)^2 + \left(y_1 - y_2\right)^2 + \left(z_1 - z_2\right)^2} \tag{35}$$

…where (x_1, y_1, z_1) and (x_2, y_2, z_2) are the Cartesian coordinates of the two ends of a string.

The shortening of the floating masts are usually very small regarding the axial deformation of the other bars of the structure. If we consider negligible the mast shortening, we can define the initial shortening of the spoke's strings by means of a direct calculation (36):

$$\Delta L_{0,i} = L_i \left(\frac{P_i \sqrt{\left(1 - k\varepsilon_{y,c}\right)^2 \left(\left(x_1 - x_2\right)^2 + \left(y_1 - y_2\right)^2\right) + \left(z_1 - z_2\right)^2}}{2EA_i \left(1 - k\varepsilon_{y,c}\right) \sqrt{\left(x_1 - x_2\right)^2 + \left(y_1 - y_2\right)^2}} - \frac{L_i - \sqrt{\left(1 - k\varepsilon_{y,c}\right)^2 \left(\left(x_1 - x_2\right)^2 + \left(y_1 - y_2\right)^2\right) + \left(z_1 - z_2\right)^2}}{L_i} \right) \tag{36}$$

… where A_i is the area of the cross section of a string of the spoke.

2.7. Synopsis of the design procedure

To recapitulate: First, we have defined the shape of the outer polygon which has equal sides and is inscribed in a super-ellipse. Secondly, we have defined the shape of the inner polygon and the arrangement of the spokes, and we have calculated the in-plane tension forces N_i and P_i on all the inner polygon's bars and also on the spokes. These two processes require iterative calculations. Thirdly, we have calculated the in-plane displacements δ_i of all the structure nodes according to the in-plane homothetic deformation, and we have defined the necessary pre-stressing, introduced by means of initial shortenings, for this deformation to take place. All these processes of iterative and direct calculations can be automated by programming in a computer-aided design tool.

Based on the resulting model, it will be necessary to analyze the structure taking into account the total loads, i.e. self-weight, thermal loads and live loads from wind and snow, in addition to the pre-stressing. In this analysis, it will be verified if an increase in the cross sections sizing and/or in the pre-stressing forces is necessary. At all events, this increase would not alter the in-plane design of the spoke wheel nor relative distribution of the tension forces due to the pre-stressing.

We show bellow a synopsis diagram of the in-plane design procedure of non-circular triangulated tensile spoke wheels (figure 11).

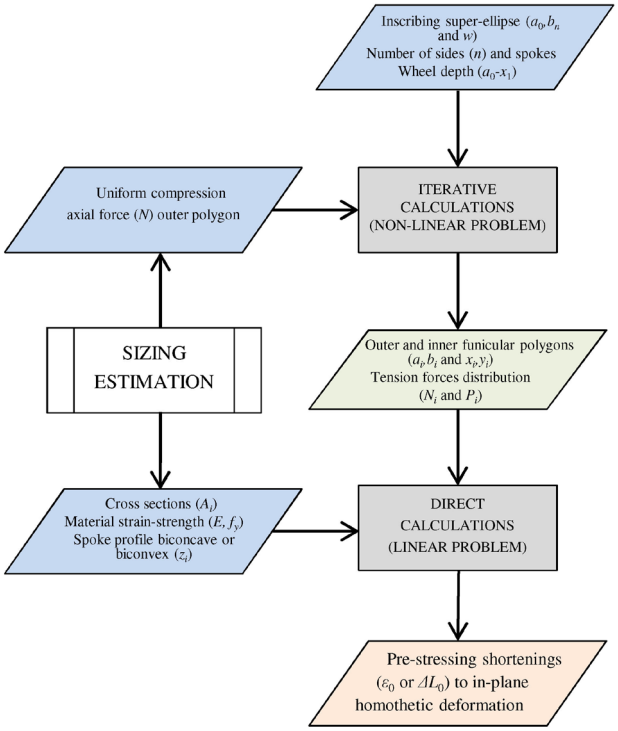

Figure 11: *Synopsis of the procedure for in-plane design of non-circular triangulated tensile spoke wheels*

2.8. Testing model

In order to test if the structure's behaviour conforms to the behaviour predicted by our in-plane design procedure for non-circular wheels, we have developed a testing model in a structural analysis software. Thus, we have considered a one-outer-polygon-two-inner-polygons-spoke-wheel structure. The in-plane design of this structure has been defined based on the procedure described above. We have started from an inscribing super-ellipse with a_0=50 m, b_n=45 m and w=2.25, and the parameters n=6 and x_1=27.5 m. Also, an uniform axial compression force N=2196.52 KN on the outer polygon has been assumed. This force corresponds to an utilisation ratio k=0.40 of a tubular cross-section 406.4x12.5 the area of which is A=15468 mm^2 of steel, where $f_{y,c}$=355 N/mm^2 and E=2.10·10^5 N/mm^2. The cross section of the tensile bars have diameters between 16 and 50 mm, and they are made of steel with $f_{y,t}$=1000 N/mm^2.

We have considered a simple spoke's profile composed of two strings, top and bottom, from the vertex of the outer polygon to the vertices, top and bottom, of the inner polygons. Thus, there are twenty four vertical floating masts between the vertices of the inner polygons. The length of these masts is 9 m and they are symmetrical regarding the horizontal plane of the outer polygon.

The resulting design and the shortenings of the tensile bars have been considered in the analysis model of the software *Autodesk Robot Structural Analysis*. This model behaves exactly as predicted by the method developed in this paper. I.e., the compression axial force is uniform on the outer polygon (figure 12a) and the deformation is a homothetic shape of the not deformed spoke-wheel (figure 12b). Then we have considered a 50% increase in the pre-stressing level (figures 12c and 12d).

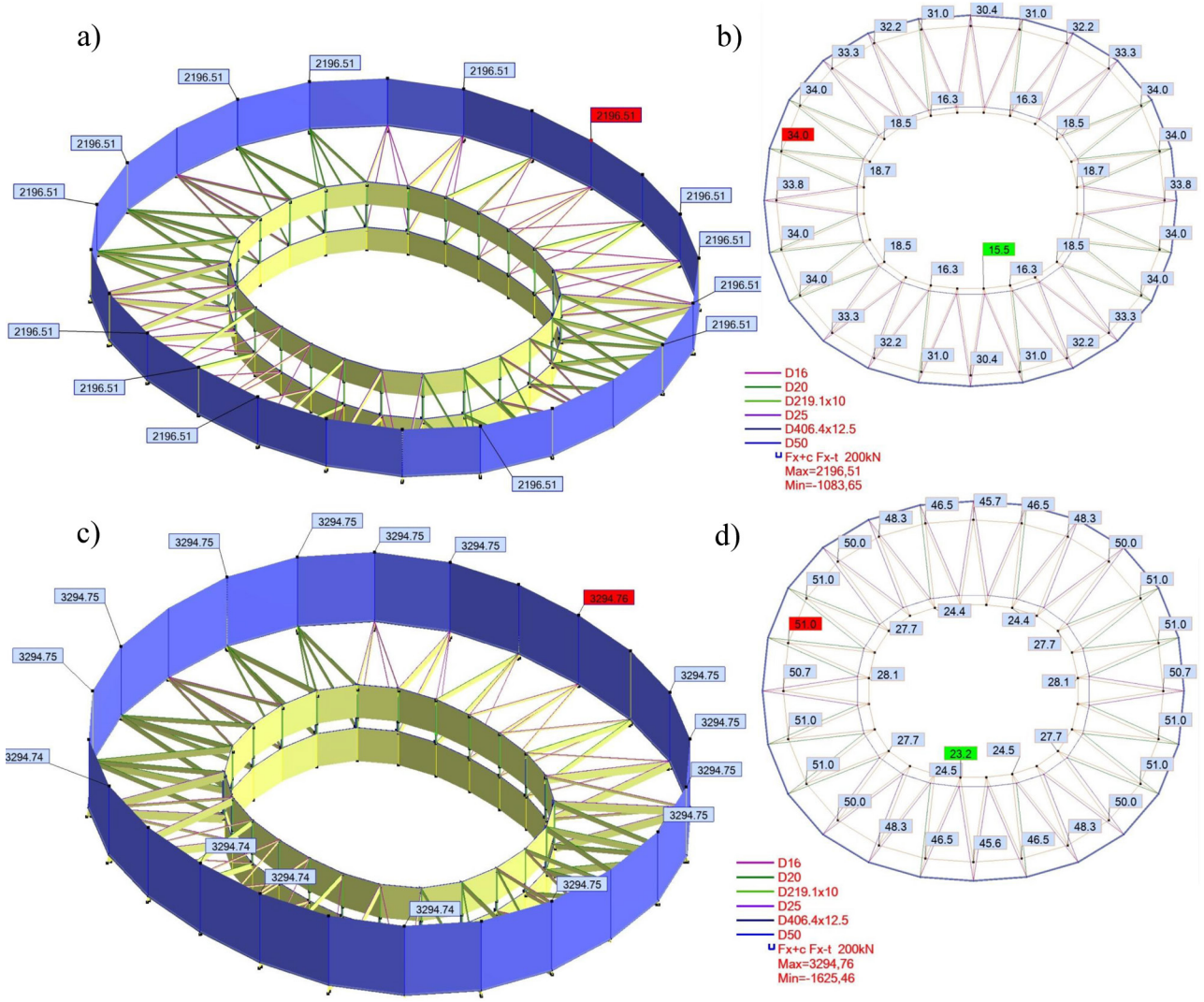

Figure 12: *Testing model analysis of a non-circular spoke wheel: a) Uniform compression forces in KN on the outer polygon resulting from the pre-stressing shortenings of the spokes and inner polygon; b) homothetic deformation with displacements in mm resulting from the pre-stressing shortenings of the spokes and the inner polygon; c) and d) uniform compression forces on the outer polygon and homothetic deformation resulting from a 50% increase in the pre-stressing level*

3. CONCLUSIONS

This paper describes a new in-plane design of a triangulated tensile spoke wheel which is inscribed in a non-circular curve with two perpendicular symmetry axes. There is also a procedure for defining the geometric shape and the pre-stressing forces.

In the resulting structure, taking into account the pre-stressing shortenings of the spokes and the inner polygons, the outer ring is a polygon with equal sides which behaves like a funicular polygon subject to uniform compression forces. Thus, the sizing conditions of the outer polygon are equated to the forces which would be present on a structure of the same type but inscribed in a circle, i.e., same buckling length and same axial force in all its bars.

We have also determined the scope of the procedure by defining the geometrical limits to obtain a viable structure. In this way, we have defined the maximum depth along the *X*-axe of the wheel that we can obtain from a combination of initial parameters.

All the processes of the design procedure described in this paper can be automated by programming in a computer-aided design tool. Owing to this, we believe this paper can be a valuable tool to obtain very optimised designs for this type of structures.

REFERENCES

[1] Yao YL, Dong SL and Ma GY, "Configuration, classification and development of large-span annular tensile cable-truss structures," *Advanced Materials Research*, vol. 255, pp. 225-229, 2011. (DOI: 10.4028/www.scientific.net/AMR.255-260.225).

[2] Göppert K, "Interdisziplinäres Entwerfen von Stadien: Unter großen Dächern," *Bautechnik*, vol. 89-10, pp. 694-700, 2012. (DOI: 10.1002/bate.201200049).

[3] Castro G and Levy M, "Analysis of the Georgia Dome cable roof," in *Proceedings of the 18th Conference of Computing in Civil Engineering and Geographic Information-Systems Symposium 1992*, *Dallas, TX, US, June 7-9, 1993*, BJ Goodno and JR Wright, Eds. ASCE, 1993. pp. 1-4.

[4] Göppert K and Stein M, "A Spoked Wheel Structure for the World's largest Convertible Roof–The New Commerzbank Arena in Frankfurt, Germany," *Structural Engineering International*, vol. 17-4, pp. 282-287, 2007. (DOI: 10.2749/101686607782359155).

[5] Bradshaw R, Campbell D, Gargari M, Mirmiran A and Tripeny P, "Special structures: past, present, and future," *Journal of Structural Engineering*, vol. 128-6, pp. 691-709, 2002. (DOI: 10.1061/(ASCE)0733-9445(2002)128:6(691)).

[6] Kim H, "Structural performance of spoke wheel roof system," Master dissertation, Department of Civil and Environmental Engineering, Massachusetts Institute of Technology, Cambridge, 2017.

[7] Schlaich Bergermann Partner, "Stadia & Arenas," in www.sbp.de/en/projects (accessed 18 August 2022).

[8] Bergermann R and Göppert K, "Das Speichenrad Ein Konstruktionsprinzip für weitgespannte Dachkonstruktionen," *Stahlbau*, vol. 69-8, pp. 595-604, 2000. (DOI: 10.1002/stab.200002200).

[9] Majowiecki M, Pinardi S, Berti G and Patruno L, "Upgrading the spoke wheel stadium roof concept," *Journal of the International Association for Shell and Spatial Structures*, vol. 60, pp. 249-256, 2019. (DOI: 10.20898/j.iass.2019.202.038).

[10] Martín-Sáiz R, "Diseño de anillos de compresión no circulares y distribución óptima de fuerzas en el plano," Ph.D. dissertation, Departamento de Tecnología de la Arquitectura, Universitat Politècnica de Catalunya, Barcelona, 2015.

[11] Tellier X, Douthe C, Hauswirth L and Baverel O, "Funicularity of conics," *Acta Mechanica*, vol. 232, pp. 3179-3191, 2021. (DOI: 10.1007/s00707-021-02987-6).

[12] Beghini A, Beghini LL, Schultz JA, Carrion J and Baker WF, "Rankines's Theorem for the design of cable structures," *Structural and Multidisciplinary Optimization*, vol. 48, pp. 877-892, 2013. (DOI: 10.1007/s00158-013-0945-2).

[13] Lachauer L and Block P, "Interactive equilibrium modeling," *International Journal Space Structures*, vol. 29-1, pp. 25-37, 2014. (DOI: 10.1260/0266-3511.29.1.25).

[14] Takahashi K and Ney L, "Advanced form finding by constraint projections for structural equilibrium with design objectives," in *Proceedings of the IASS Symposium 2018, Boston, MA, US*, *July 16-20, 2018*, C Mueller and S Adriaenssens, Eds. IASS, 2018. pp. 1-8.

[15] D'Acunto P, Jasienski J-P, Ohlbrock P, Fivet C, Schwartz J and Zastavni, D, "Vector-based 3D graphic statics: A framework for the design of spatial structures based on the relation between form and forces," *International Journal of Solids and Structures*, vol. 167, pp. 58-70, 2019. (DOI: 10.1016/j.ijsolstr.2019.02.008).

[16] Li Q, Shepherd P, Gilbert M and He L, "Rationalization of layout optimization result by updating discretization of the design domain," in *Proceedings of the IASS Symposium 2019, Barcelona, Spain*, *October 7-10, 2019*, C Lázaro, K-U Bletzinger and E Oñate, Eds. IASS, 2019. pp. 1-8.

[17] Pastrana P, Ole Ohlbrock P, Oberbichler T, D'Acunto P and Parascho S, "Constrained form-finding of tension-compression structures using automatic differentiation,"

Computer-Aided Design, vol. 155, pp. 103435, 2023. (DOI: 10.1016/j.cad.2022.103435).

[18] Boom I, "Tensile-compression ring. A study for football stadia roof structure," Master dissertation, Department of Building Engineering, University of Technology Delf, 2013.

[19] Herning G and Kim H, "Relationship between geometric parameters and structural efficiency of spoke wheel roof system," in *Proceedings of IASS Symposium 2018, Boston, MA, US, July 16-20, 2018*, C Mueller and S Adriaenssens, Eds. IASS, 2018. pp. 1-6.

[20] Tamai H, "On a family of equilibrium geometry of a spoke-wheel structure: Geometric approach to form finding of a spoke wheel system," in *Proceedings of IASS Symposium 2018, Boston, MA, US, July 16-20, 2018*, C Mueller and S Adriaenssens, Eds. IASS, 2018. pp. 1-8.

[21] Tamai H, "Geometric approach to form finding of a spoke wheel system: Mathematical explanations," in *Proceedings of the IASS Symposium 2019, Barcelona, Spain, October 7-10, 2019*, C Lázaro, K-U Bletzinger and E Oñate, Eds. IASS, 2019. pp. 1-9.

[22] Tamai H and Takahashi K, "The extended method for form finding of a spoke wheel system in light of graphic statics," in *Proceedings of the IASS Symposium 2022, Beijing, China, September 19, 2022*,. IASS, 2022. pp. 1-12.

[23] Nie R, He B, Hodges DH and Ma X, "Form finding and design optimization of cable network structures with flexible frames," *Computers and Structures*, vol. 220, pp. 81-91, 2019. (DOI: 10.1016/j.compstruc.2019.05.004).

[24] Xue S, Li X and Liu Y, "Advanced form finding of cable roof structures integral with supporting frames: Numerical methods and case studies," *Journal of Building Engineering*, vol. 60-15, pp. 105204, 2022. (DOI: 10.1016/j.jobe.2022.105204).

[25] Iz S, "Pretensioning cable roof systems Besiktas Stadium design principles," *Jounal of Innovations in Civil Engineering and Technology*, vol. 1-2, pp. 75-97, 2019.

[26] Liu R, Xue S, Sun G and Li X, "Formulas for the derivation of node coordinates of annular crossed cable-truss structure in a pre-stressed state," *Jounral of the International Association of Shell and Spatial Structures*, vol. 55-4, pp. 223-228, 2014.

[27] Liu R, Xue S, Cao J, Li X and Liu Y, "Analysis on single-layer hyperbolic cable net structure schemes of stadium roof," *Journal of Building Structures*, vol. 43-9, pp. 269-276, 2022. DOI: 10.14006/j.jzjgxb.2021.0247.

[28] Hu Z, Wang J, Zhao J and Chen Y, "Experimental study on wheel-spoke crossed cable structures," *Advances in Structural Engineering*, vol. 21-15, pp. 2340-2355, 2018. (DOI: 10.1177/1369433218773456).

[29] Geiger D. "Roof Structure". US Patent 4,736,553. 1988.

[30] Fuller RB, Applewhite EJ. *Synergetics. Exploration in the geometry of thinking*. New York: Macmillan Publishing Co. 1975.

[31] Weisstein EW, "Superellipse," in *Mathworld Wolfram*,www.mathword.wolfram.com/Superellipse (accessed 25 July 2022).

[32] Demidovich BP and Maron IA, *Fundamental of computational mathematics*. Moscow: Fizmatgiz, 1963.

[33] Cabello A, "Predimensioning sub-space for spoke-wheel roofs," *Journal of the International Association for Shell and Spatial Structures,* vol. 59-2, pp. 119-130, 2018. (DOI: 10.20898/j.iass.2018.196.875).